Applied Catalysis B: Environmental 304 (2022) 121003

Contents lists available at ScienceDirect

Applied Catalysis B: Environmental

journal homepage: www.elsevier.com/locate/apcatb

Advanced treatment of landfill leachate using integrated coagulation/ photo-Fenton process through in-situ generated nascent Al^{3+} and H_2O_2 by Cl, N co-doped aluminum-graphite composite

Yong Liu [a], Yong Chen [a], Yufeng Da [a], Fei Xie [b], Jianlong Wang [c,*]

[a] College of Chemistry and Materials Science, Sichuan Normal University, Chengdu 610066, PR China
[b] Sichuan Deep-Blue Environmental Technologies Co., Ltd, Chengdu 610060, PR China
[c] Laboratory of Environmental Technology, INET, Tsinghua University, Beijing 100084, PR China

ARTICLE INFO

Keywords:
Landfill leachate
Coagulant
Advanced oxidation process
Refractory organic pollutant
Advanced treatment

ABSTRACT

Herein, we report an integrated coagulation/ photo-Fenton (CPF) process for advanced treatment of mature landfill leachate using nascent aluminum ions as coagulant and hydrogen peroxide (H_2O_2) as oxidant for Fenton reaction, which were in-situ produced by a novel chlorine and nitrogen co-doped aluminum-graphite (Cl, N-Al-Gr) composite. The coagulation of the MBR-treated landfill leachate was performed by nascent aluminum ions generated in Cl, N-Al-Gr/O_2 system; and the resulting coagulation effluent was treated by photo-Fenton oxidation in the presence of ultraviolet (UVA). The Cl, N-Al-Gr composite exhibited excellent performance for in-situ H_2O_2 production (813.9 mg/L). The humic substances in landfill leachate could promote the cycle of Fe^{3+}/Fe^{2+}, and the removal efficiency of total organic carbon (TOC) and color was 88.1% and 97.6%, respectively under the optimized condition. The current study suggested that "coagulation + Fenton" process using nascent Al^{3+} as coagulant and in-situ generated H_2O_2 for Fenton oxidation could be a new way for wastewater treatment.

1. Introduction

Landfill leachate is produced in the landfill process of municipal solid waste (MSW), which is a highly complex wastewater and contains high concentrations of refractory organic pollutants, salt compounds and other toxic contaminants [1–3], which makes it be one of the main pollution sources of groundwater and surface water [4]. Various anaerobic/aerobic biological treatment processes have been used to remove organic pollutants in landfill leachate [5]. However, a lot of refractory organic pollutants include humus and toxic organics such as aromatics, bisphenols, phthalate esters, etc. [6–9] have been detected in the effluent from biological treatment of leachate, especially, in leachate from old landfill. Therefore, the removal of refractory organic pollutants in landfill leachate has attracted more and more attention.

Several physicochemical methods have been used to remove refractory organic pollutants in landfill leachate, including electrochemical advanced oxidation [10,11], reactive electrochemical membranes [12], adsorption [7,13], coagulation [3,14], micro-electrolysis [15], advanced oxidation processes (AOPs) [16], etc. Among them, coagulation and AOPs have gained increasing attention due to their simplicity and high efficiency. However, the removal of refractory organic pollutants by coagulation alone is very limited. Many coagulation processes only remove 30–50% COD [17,18]. AOPs can mineralize refractory organics directly or converted it into biodegradable substances [14,19,20].

Fenton oxidation has been applied for the treatment of landfill leachate [21,22]. The coagulation integrated with Fenton process is considered as an emerging strategy for removal of refractory organic pollutants in landfill leachate [22]. In the conventional coagulation -Fenton oxidation process, there are two disadvantages: (1) It needs additional coagulant and hydrogen peroxide (H_2O_2), which will increase the cost of the agent and cause the security risk of H_2O_2 transportation and storage [23]; (2) The catalytic efficiency of Fe^{2+} for the decomposition of H_2O_2 is low due to that the key rate-limiting step is the effective conversion the Fe^{3+} into Fe^{2+} [24]. Therefore, aiming at in-situ generation of coagulant and H_2O_2, the development of more convenient and effective coagulation-Fenton oxidation process to treat landfill leachate is urgently required.

The in-situ production of H_2O_2 by electro-catalysis and the micro-electrolysis have recently gained wide attention owing to its

* Correspondence to: Energy Science Building, INET, Tsinghua University, Beijing 100084 PR China.
E-mail address: wangjl@tsinghua.edu.cn (J. Wang).

https://doi.org/10.1016/j.apcatb.2021.121003
Received 12 October 2021; Received in revised form 1 December 2021; Accepted 6 December 2021
Available online 8 December 2021

fascinating advantages and various potential applications in wastewater. This thought made us aware of the benefits of the corrosion electrochemistry strategy for in-situ production of H_2O_2. Particularly, in our recent works, a series of aluminum-carbon (Al-C) composites were prepared by high-energy ball milling combined with sintering process [1,25,26]. The Al-C composites could activate O_2 to produce nascent aluminum ions and H_2O_2 in-situ by micro-electrolysis process [23,27]. In particular, the Al-C-N/O_2 composite could greatly improve the production efficiency of H_2O_2 (over 2000 mg/L at the Al-C-N dosage of 8 g/L) [1], which provides the possibility to the treatment of landfill leachate by coagulation -Fenton oxidation without additional coagulant and H_2O_2.

$$2\ \text{Al-C-N} + 3\ O_2 + 6\ H^+ \rightarrow 2Al^{3+} + 3\ H_2O_2 \quad (1)$$

However, the synthesis of Al-C-N composites required the pretreatment of aluminum powder by high energy ball-milling process to eliminate the oxide film on aluminum surface and obtain nano aluminum, which leads to the high energy consumption and difficult storage of Al-C-N composites. In the sintering process of many metallurgical industries, some alkali metal salts are often added to the complex oxide minerals to transform the insoluble minerals into soluble molten salts, which can remove the impurities in the minerals [28,29]. Learn from this idea, the addition of alkali-chloride in the micro aluminum powder will convert the aluminum oxide into aluminum salt in the sintering process, which will not only eliminate the adverse effect of oxide film on the aluminum surface on the synthesis and properties of Al-C-N, but also promote the corrosive pitting of the Al-C-N in aqueous solution by chloride ions (Cl^-). Therefore, the Al-C-N synthesized by the assistance of alkali-chloride without pre-treatment of micro aluminum powder will be have great potential to application for the wastewater treatment due to its more convenient synthesis.

It was reported that polycarboxylic acids, such as oxalic acid, citric acid and fulvic acid/humic acid, can rapidly transform Fe^{3+} into Fe^{2+} under the photo irradiation by intramolecular ligand-to-metal charge transfer (LMCT) mechanism, and many reactive oxygen species (ROSs) will be generated in the system via Eqs. (2)–(4) [30–34].

$$Fe(OH)^{2+} + hv \rightarrow Fe^{2+} + \bullet OH \quad (2)$$

$$Fe(OOCR)^{2+} + hv \rightarrow Fe^{2+} + CO_2\bullet + R\bullet \quad (3)$$

$$R\bullet + O_2 + H_2O \rightarrow R1 + CO_2 + O_2\bullet^-/\bullet OOH \quad (4)$$

The photochemical properties of hematite-oxalate system were investigated [35], the results showed that some ROSs, such as $CO_2\bullet^-$, $O_2\bullet^-$ / •OOH and •OH were formed by the photolysis of Fe(III)-oxalate complexes and the photo-degradation, and mineralization of sulfadimidine (5 mg/L) reached 95% and 59% within 2 h using hematite-Ox system. Hong et al. [36] investigated the photo-degradation of atrazine in the presence of Fe^{3+}-montmorillonite and Suwannee river fulvic acid (SRFA) in aqueous solution, and they found that both •OH and singlet oxygen were responsible for the degradation process in the Fe^{3+}-montmorillonite /SRFA hybrid system. There are large amounts of humic substances, such as humic acid and fulvic acid in the effluent from the coagulation treatment of landfill leachate [3,14]. Therefore, it can be inferred that the LMCT process from the humic substances to Fe^{3+} may be occurred under the involvement of Fe^{3+} and ultraviolet light (UVA). Besides, the H_2O_2 can be decomposed directly to •OH [11] and its utilization efficiency can be further improved. Therefore, if the Fe^{3+} and ultraviolet light are introduced into the coagulation effluent of landfill leachate, it can not only improve the utilization efficiency of H_2O_2, but also increase the oxidation species in the system.

Herein, a novel coagulation-photo Fenton process derived from the in-situ production of nascent aluminum ions and H_2O_2 (denoted as hybrid CPF process) was employed to remove the refractory organic pollutants in the mature landfill leachate. The in-situ production of aluminum ions and H_2O_2 was obtained from O_2 activation by a novel chlorine and nitrogen co-doped aluminum-graphite (Cl, N-Al-Gr) composite, which was synthesized via a simple mix-sintering process. In this hybrid CPF process, the refractory organic pollutants were first removed by Cl, N-Al-Gr/O_2 coagulation process and the H_2O_2 was produced in-situ at the same time, and then the residual refractory organic pollutants were further removed by photo-Fenton oxidation process via adding Fe^{2+} and ultraviolet light into the effluent from Cl, N-AlGr /O_2 coagulation process. The effect factor and mechanism of the removal of refractory organic pollutants are discussed. Besides, the performance of the activation of O_2 by Cl, N-Al-Gr composite for the H_2O_2 production was examined. Our work will provide a new way for the treatment of landfill leachate by "coagulation + Fenton" hybrid process.

2. Materials and methods

2.1. Chemicals, materials, and leachates

Aluminum metal powders (200–400 mm, 2.700 g/cm^3) and graphite (Gr) powders were purchased from Kelong Chemical Reagent Factory (Chengdu, China), while melamine, glycine, polyethylene glycol (PEG) 4000 were obtained from Aladdin Chemistry. Potassium chloride, H_2O_2, titanium potassium oxalate, methyl viologen (MV), tert-butanol (TBA), bisphenol-A, and benzoquinone (BQ) were obtained from the National Medicines Co., Ltd., China. All chemicals were all analytical grade or higher and used without further purification. Ultra-pure water (resistance > 18 MΩ/cm) prepared by using Milli-Q system (Millipore Co., USA) was used in all experiments.

The leachate samples used in this study were obtained from landfill leachate effluent of the membrane bioreactor (MBR) treatment system generated from an old municipal solid waste landfill in Meishan city, China. The raw leachate was pre-treated by a mesophilic anaerobic/aerobic MBR process. Therefore, the leachate sample was denoted as MBR effluent, which was immediately preserved in a refrigerator at 4^0 C to minimize the biological and chemical reactions. The MBR effluent had a dark brown color, and the general characteristics were as follows: pH 7.10 ± 0.2, Cl^- 0.135 mol/L, COD 1302.8 ± 16 mg/L, TOC 488.5 ± 16 mg/L, BOD_5 122 ± 11.8 mg/L and the ratio of BOD_5/COD about 0.17 ± 0.1, indicating the low biodegradability of the MBR effluent and containing a lot of refractory organic pollutants.

2.2. Materials synthesis and characterization

The synthesis of Cl, N-Al-Gr composite was carried out by a simple mix-sintering process. A typical synthesis process was as follows. Firstly, 1.5 g aluminum powders, 0.15 g graphite powers, 0.15 g melamine, 0.15 g glycine, and 0.1 g potassium chloride were mixed and pulverized to 200 mesh. The mixture and 1.11 g polyethylene glycol 4000 were added into a cylindrical glass container with cover and magnetic stirred for 3 min at the temperature of 60 ℃, stirring speed of 300 rpm and an argon gas protection. After cooling into room temperature, the obtained precursors were transferred to a porcelain boat and sintered in a tube furnace at 700 ℃ for 60 min with an argon gas flow rate of 60 mL/min and cooled into room temperature to obtain Cl, N-Al-Gr composite (Scheme 1).

Cl, N-Al-Gr composite was characterized by scanning electron microscopy (SEM, JSM-7500 F, Jeol, Japan), energy-dispersive spectrometer (EDS, XMax50, Oxford, England), X-ray diffraction (XRD, BrukeD8 Adv., Germany), and X-ray photoelectron spectroscopy (XPS, Thermo Fisher Scientific K-Alpha, USA).

The oxygen reduction reaction (ORR) performance was investigated by a CHI 760E electrochemical work station (Shanghai Chenhua, China) in a conventional three-electrode system at 25 ℃. The working electrode, counter electrode, and reference electrode were graphite sheet (10 *15 mm), platinum electrode and saturated calomel electrode (SCE), respectively. The working electrode was prepared according to follow: the catalyst ink was prepared by an ultrasonic mixture of

Scheme 1. synthesis of Cl, N-Al-Gr composite by mix-sintering process.

0.06 mg of catalyst and 0.6 mL of Nafion solution, which was prepared by mixing 0.4 mL of Nafion with 0.2 mL of isopropanol. Then, the prepared catalyst ink was dropped into a graphite sheet and dried.

The Tafel tests were carried out in the potential range of − 1.6–0.4 V at a scanning rate of 0.01 V/s. Electrochemical impedance spectroscopy (EIS) were measured at the open circuit potential in a frequency of 0.01 Hz-1000 kHz with the amplitude of 10 mV.

2.3. Production of H_2O_2

The experiments for the H_2O_2 production on site were performed in a 250-mL glass beaker containing 150 mL of aqueous solution. The procedure was similar to our previous works [23,37]. Typically, after a known amount of Cl, N-Al-Gr was added into aqueous solution, the suspension was stirred continuously at a constant rate of 300 rpm. Then, the oxygen gas with a flow rate of 400 mL/min was put into the reactor. Prior to the experiment, the desired initial pH value of the solution was adjusted using H_2SO_4 (0.1 M) or NaOH (0.1 M) solution. Samples were taken and filtered by 0.20 μm filter membrane to determine the concentrations of the H_2O_2 at pre-set intervals time.

2.4. Coagulation integrated with photo-Fenton oxidation experiments

2.4.1. Coagulation along with H_2O_2 production from Cl, N-Al-Gr/O_2 process

Coagulation along with H_2O_2 production tests were conducted in a 250-mL glass beaker. A known amount of Cl, N-Al-Gr composite was added into 150 mL of MBR effluent after the initial solution pH was adjusted to set value with 0.1 M H_2SO_4 or NaOH solution. Then, the suspension was stirred continuously at a constant rate of 300 rpm and the oxygen gas with a flow rate of 400 mL/min was passed through the reactor to initiate reaction. After reaction for set time, the mixture solution was settled for 10 min and the supernatant was taken for the determination of TOC, H_2O_2 concentration and color. Under the optimum condition, molecular weight (MW) distribution and three-dimensional excitation and emission matrix (3D-EEM) fluorescence spectroscopy were measured before and after treatment.

2.4.2. Photo-Fenton oxidation from Fe^{2+}/UVA process

In the photo-Fenton procedure, 50 mL coagulation effluent was firstly transferred into a 100-mL quartz glass tube, then put into a photocatalytic reactor (Xujiang, Nanjing). Magnetic stirring was applied at a rotary speed of 200 rpm and a high pressure mercury lamp (main wavelength is approximately 365 nm) was used to provide UVA irradiation because it has higher energy than visible light, which can promote the photo-induced electron transfer process of iron- HA system, boosting the degradation of organic pollutants. The reaction was initiated by adding a known concentration of Fe^{2+} in the solution and the solution was irradiated at the light intensity of 50.01 mW/cm^2. At certain time intervals, 1 mL of samples was taken out and filtered by 0.22 μm membrane filters to determine the concentration of TOC, H_2O_2 and CN. The photo-Fenton oxidation experiment was also conducted twice, averaging the data. Under the optimum condition, the concentration of iron ions in solution, MW distribution and 3D-EEM fluorescence spectroscopy were measured.

2.5. Analytical methods

The H_2O_2 concentration was measured on an UV–vis spectrometer (UV-2100, Shanghai, China) at 400 nm using potassium titanium oxalate as a chromogenic reagent [1]. Total organic carbon (TOC) concentration was determined on a Multi TOC/TN Analyzer (2100, AnalytikJena. Germany). The Fe^{2+} concentration was analyzed at 510 nm using o-phenanthroline as chromogenic reagent. The concentration of bisphenol-A was determined by high performance liquid chromatography (HPLC, Agilent 1200 Series, USA). The concentration of Cl^- was measured by ion chromatograph (ICS-1100, DIONEX, USA).

Electron paramagnetic resonance (EPR) spectra of free radicals such as •OH, O_2•$^-$ and CO_2•- were recorded on a Bruker EMX nano spectrometer (Bruker, Germany) with 5, 5-dimethyl-1-pyrroline N-oxide (DMPO) as spin-strapping agent.

3D-EEM Fluorescence spectroscopy was recorded on an F-4500 fluorescence spectrophotometer (Hitachi, Tokyo, Japan) with a xenon lamp as the excitation source at the excitation wavelengths from 200 to 550 nm and scanning speed of 1200 nm/min [14,22]. Before determination, the samples were diluted by tenfold using ultra-pure water due to its high contents of organic pollutants.

The MW distribution of the samples was measured by an ultrafiltration apparatus with different MW cutoffs of 500 Da and 10 kDa. The MW fractions were characterized by TOC values of filtrate [16,22].

3. Results and discussion

3.1. The characterization of Cl, N-Al-Gr composite

SEM image, EDS spectra and EDS mapping of Cl, N-Al-Gr composite were shown in Fig. 1. The Cl, N-Al-Gr composite exhibited a sphere structure and large dispersive nano-sheets were adhered to the surface of sphere particles. The element peak at 0.25 keV confirmed the existence of Cl and the elements of Cl was evenly distributed in Cl, N-Al-Gr composite particles, suggesting that Cl successfully supported on the surface of Cl, N-Al-Gr composite particles.

As shown in Fig. 1e, the reflection peak at 26.23° assigning to Gr (JCPDS 75–1621), and peaks at 38.47°, 44.74°, 65.14°, 78.23° and 82.44° attributing to zero valent aluminum (Al^0) (JCPDS 04–0787). The peak at 28.41° was corresponded to the (200) reflection of KCl (JCPDS 73–0380), indicating the existence of Cl^- in the Cl, N-Al-Gr composite particles, which might result in the pitting corrosion of Al^0.

XPS was conducted to examine the chemical compositions of Cl, N-Al-Gr composite and the location of Cl element defect. Fig. 1d clearly confirmed the existence of Al, O, Cl, N, K and C. The N1s XPS spectrum revealed the presence of four peaks corresponding to AlN (BE = 397.3 eV), pyridine (BE = 398.3 eV), pyrrole (BE = 399.6 eV) and graphitic N (BE = 400.5 eV) [1]. The peaks at 198.0 eV and 200.2 eV in Cl 2p XPS spectra in Fig. 1f could be attributed to Cl $2p_{3/2}$ in metal chloride and Cl $2p_{1/2}$ in organic Cl, respectively [38,39], suggesting that KCl in precursors could result in the formation of organic Cl and metal chloride in Cl, N-Al-Gr composite particles. Huang, et al. [38] was also obtained the organic Cl and metal chloride in the carbon material when KCl was added in the precursors. The Cl content in Cl, N-Al-Gr composite from XPS was 3.5%, corresponding to the KCl content in precursors of

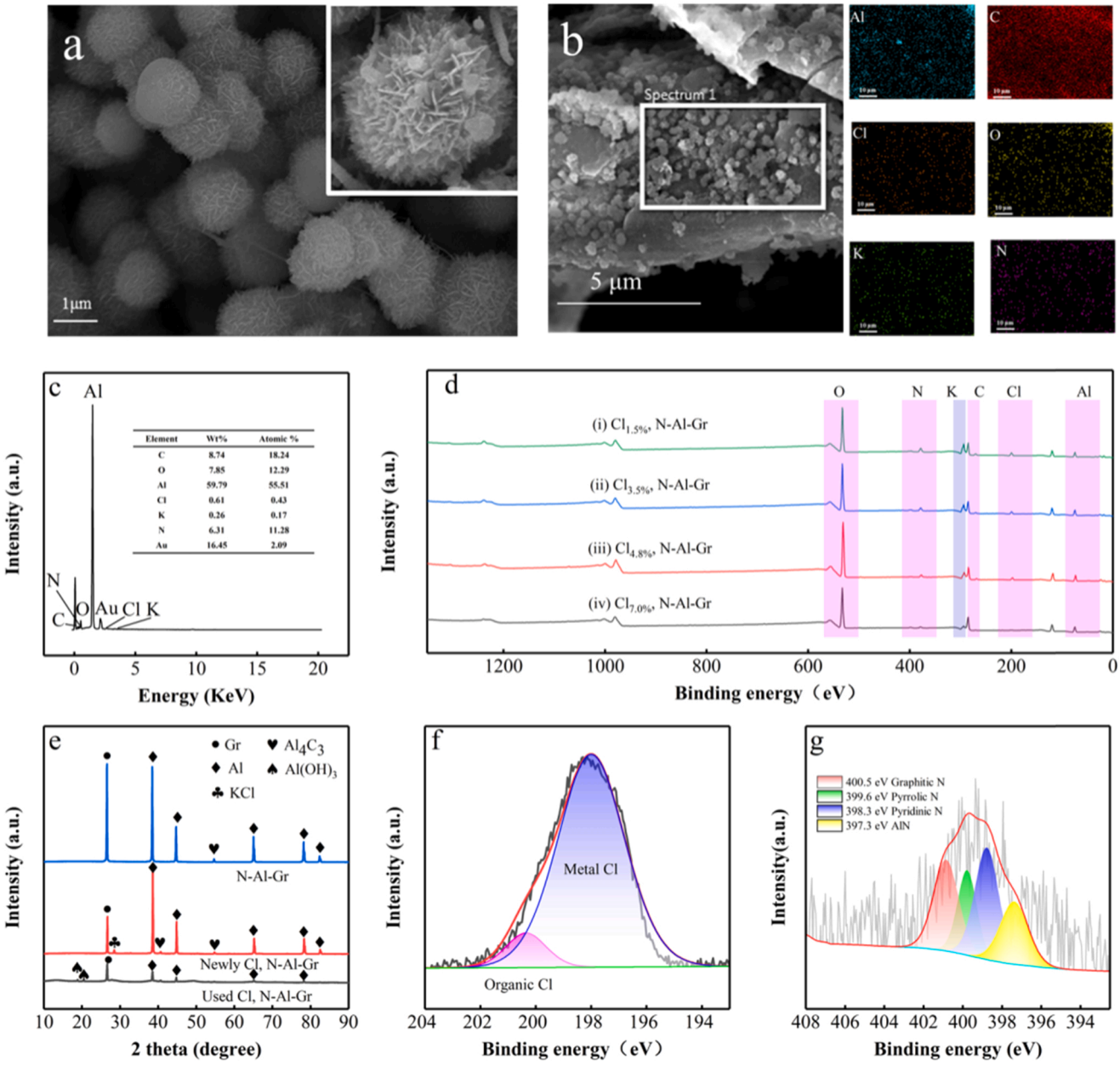

Fig. 1. SEM image of Cl, N-Al-Gr (a), EDS mapping of Cl, N-Al-Gr (b), EDS spectrum of Cl, N-Al-Gr (c), XPS full survey spectra of Cl_x, N-Al-Gr synthesized by different content KCl in precursors. i, ii, iii, and iv presented KCl content in precursors of 1.4%, 2.7%, 5.4% and 10.8%, respectively. the x presented the content of Cl in Cl_x, N-Al-Gr (d), XRD patterns of different N-Al-Gr composites (e), Cl2p deconvolution of Cl, N-Al-Gr(f), and N1s deconvolution of Cl, N-Al-Gr (g).

2.7%. The XPS of Cl, N co-doped Al-Gr composite synthesized by different KCl content in precursors were also carried out. The results showed that when the KCl content in precursors was 1.4%, 5.4% and 10.8%, the Cl content in Cl, N co-doped Al-Gr composite were 1.5%, 4.8% and 7.0%, respectively (Fig. 1d).

From above characterization results, the Cl and N were successfully co-doped in the Al-Gr particles. The successful doping of Cl and N might be due to following reasons: (1) During the sintering process, the mixture of melamine and glycine in precursors were decomposed and then generated active nitrogen species. These active nitrogen species reacted with Gr or Al, thereby nitrogen was effectively introduced as a mix (pyridine N, pyrrolic N, graphitic N and AlN). The formation mechanism of nitrogen active sites by the sintering of the mixture of nitrogenous organic precursors and carbon materials was discussed in previous works [1,40,41]. (2) In some metallurgical industries, some alkali metal salts could react with complex oxide minerals and transformed into molten salts at high temperature sintering process (28; 29).

Similar to these processes, during the sintering process, KCl in precursors interacted with the aluminum oxide on the surface of micro aluminum powder to form aluminum chloride, and then most of aluminum chloride was migrated to gas phase due to its low boiling point (178 °C). At the same time, KCl interacted with organics, part of Cl was recaptured by active carbon sites from organic pyrolysis (such as, cracking fragments, molten reaction intermediates, and so on) [38], thereby forming organic Cl. The formation mechanisms of organic Cl by the interaction KCl with organics (such as cellulose, xylan, lignin and pectin, etc.) were reported previously [38,42,43].

3.2. Production of H_2O_2 by Cl, N-Al-Gr composite through O_2 activation

3.2.1. Role of Cl-doping

Fig. 2a shows the accumulation concentration of H_2O_2 from the O_2 activation by Cl_x, N-Al-Gr composite at the dosage of Cl_x, N-Al-Gr 2 g/L and the initial pH 9. X presents the Cl content in Cl_x, N-Al-Gr from XPS result. The accumulation concentration of H_2O_2 in Al-Gr-N/O_2 system was only 61.9 mg/L within 120 min, while the accumulation concentration of H_2O_2 in $Cl_{1.5\%}$, N-Al-Gr/O_2 system was 369.7 mg/L, indicating that the production of H_2O_2 was accelerated by the doping of Cl. However, when the Cl content in Cl_x, N-Al-Gr increased from 3.5% to 7.0%, the accumulation concentration of H_2O_2 deceased from 813.9 mg/L to 292.9 mg/L. Therefore, Cl, N-Al-Gr composite with Cl content of 3.5% that was synthetized by using KCl as one of the precursors and the content of KCl in precursors of 2.7%, was selected in the following experiments.

Fig. 2b shows that the EIS of Cl_x, N-Al-Gr were single capacitive reactance arc, suggesting that the electrode reaction was controlled by electrochemical reaction. The radius of capacitive arc reflected the impedance of corrosion product film and the performance of protecting matrix [44]. The lower the radius of capacitive arc means the better the corrosion ability of the electrode system [45]. When the Cl content in Cl_x, N-Al-Gr from 0% to 7.0%, the radius of capacitive reactance arc decreased significantly, suggesting that higher Cl-doping content exhibited higher facilitation to the aluminum corrosion.

In order to further discuss the role of Cl-doping, Tafel tests were examined. As shown in Fig. 2c, with the increase of Cl-doping content, the Tafel slopes decreased in turn, which indicated that the increase of Cl-doping content accelerated the breakdown of passive film and promoted the corrosion of aluminum.

During the reaction, the concentration of Cl^- that released into the solution was determined. When the Cl content in Cl_x, N-Al-Gr of 1.5%, 3.5%, 4.8% and 7.0%, the released Cl^- in solution was 0.61, 1.21, 3.71 and 8.57 mmol/L, respectively. The released Cl^- was lower than that in the Cl_x, N-Al-Gr particles, suggesting that some Cl^- was fixed in the framework of Cl_x, N-Al-Gr, which favored the electron transfer in the aluminum corrosion process.

In order to explore the contribution of Cl^- in solution and in solid composite to the performance of Cl, N-Al-Gr for H_2O_2 production, the Cl, N-Al-Gr was washed by ultrapure water until to no Cl^- detection. The washed Cl, N-Al-Gr was used to produce H_2O_2 by ORR process. Fig. 2d showed that the accumulation concentration of H_2O_2 (533.8 mg/L) within 120 min in Cl, N-Al-Gr after washing/O_2 system was slightly lower than that in Cl, N-Al-Gr/O_2 system (813.9 mg/L), indicating that the contribution of Cl^- in solution to the H_2O_2 productions by Cl, N-Al-Gr/O_2 process was limited. In order to explore the action of Cl in the composite to performance of Cl, N-Al-Gr, the H_2O_2 productions by Cl, N-Al-Gr/O_2, N-Al-Gr/O_2 and N-Al-Gr/Cl^-/O_2 system were investigated, respectively. Fig. 2d showed that the N-Al-Gr has poor performance for production of H_2O_2. When N-Al-Gr was put into a solution with Cl^- concentration of 70.0 mg/L, the accumulation concentration of H_2O_2 within 120 min (432.9 mg/L) was lower than that in Cl, N-Al-Gr/O_2 system (813.9 mg/L), also suggesting the limited contribution of Cl^- in solution to the improvement of performance of Cl, N-Al-Gr.

In order to explain this phenomenon, the XRD pattern of Cl, N-Al-Gr was compared with that of N-Al-Gr (Fig. 1e). A new reflection (40.14°) of Al_3C_4 was observed in the XRD pattern of Cl, N-Al-Gr compared with that of N-Al-Gr. According to the Scherrer formula, it was calculated that

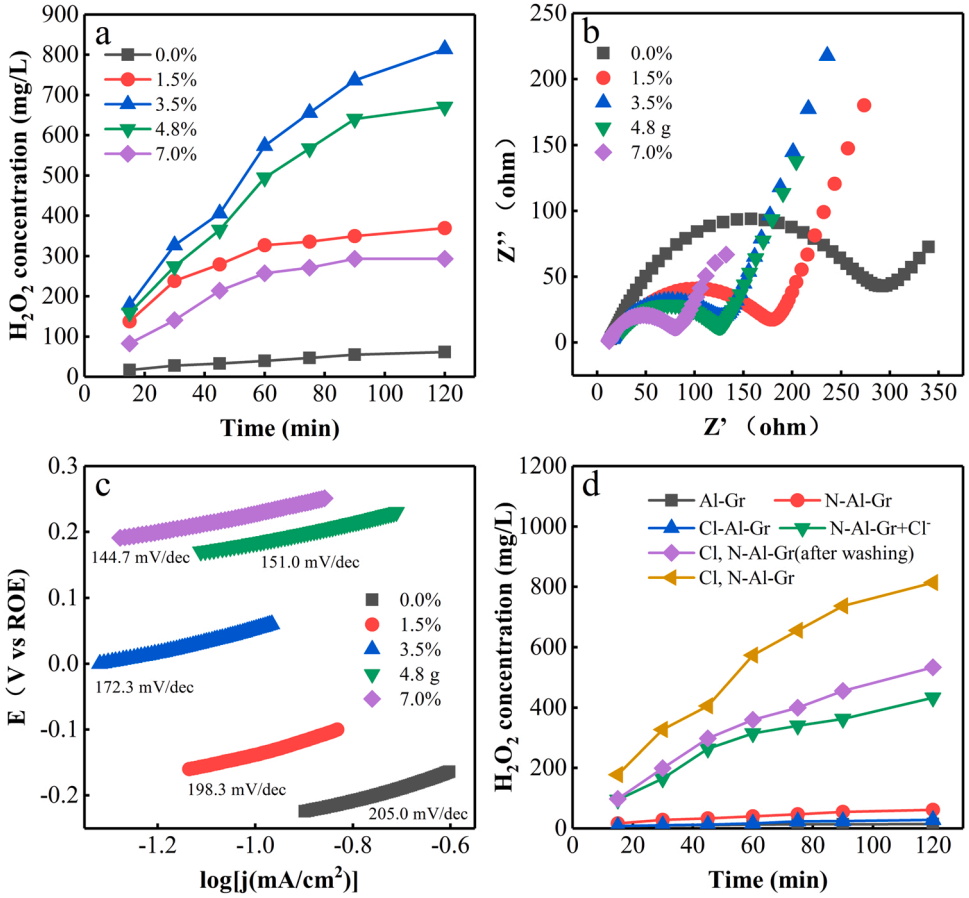

Fig. 2. Effect of Cl^- content in precursors on H_2O_2 production. Reaction condition: initial pH = 9, T = 20 °C, composites dosage = 2 g/L, O_2 flow rate = 400 mL/min. (a), EIS of the Al-Gr-N and Cl_x, N-Al-Gr (b), Tafel curves of the Al-Gr-N and Cl_x N-Al-Gr in O_2-saturated PBS at a scan rate of 10 mV/s (c) and H_2O_2 concentration in different systems. Reaction condition: initial pH = 9, T = 20 °C, composites dosage = 2 g/L, O_2 flow rate = 400 mL/min (d).

the particle size of Al_3C_4 was 40.8 nm in Cl, N-Al-Gr while it was 100.3 nm in N-Al-Gr. More crystal planes and smaller particles of Al_3C_4 meant to higher activity. Besides, the ratio of peak intensity of Al at 38.47° to peak intensity Gr at 26.61° in Cl, N-Al-Gr (2.16) was higher than that in N-Al-Gr (0.97), suggesting that a more active sites of Al were exposed in the Cl, N-Al-Gr. Above results indicated that the Cl^- in precursor is of great significance in the synthesis of Cl-doped composites. It could lead to the Cl-doped composites with higher activity of Al_3C_4 and more exposed Al active sites, which would accelerate the corrosion of aluminum.

Based on above results, it could be concluded that of Cl-doping played two roles in the performance of Cl_x, N-Al-Gr. On one hand, it accelerated the corrosion of aluminum, which was confirmed by EIS and Tafel tests results. It might be owing to:(1) Cl^- could promote the pitting corrosion of aluminum; (2) during the reaction, the Cl^- shed from the Cl_x, N-Al-Gr, which exposed more active sites of aluminum or formed some crevices, inducing crevice corrosion [46,47]; (3) metal chloride in Cl_x, N-Al-Gr could increase the charge transfer [48,49]. The formation of organic Cl was found in the Cl_x, N-Al-Gr. However, the specific components and functions will be investigated in our further work. The facilitation of aluminum corrosion by Cl-doping led to the high accumulation concentration of H_2O_2.

On the other hand, too high Cl-doping content inhibited the generation of H_2O_2, which might be owing to two reasons: (1) during the pitting corrosion of aluminum, Cl^- would migrate and accumulate in the pitting hole by autocatalytic effect of occluded corrosion cell, which promoted the hydrolysis of aluminum ions and increases the concentration of proton in the pitting hole. Too high Cl-doping content might make excessive Cl^- enter the pitting hole and produce excessive proton, which would bring about hydrogen-type corrosion of aluminum when the O_2 in the pitting hole was exhausted, reducing the aluminum content involved in O_2 activation; Moreover, in the pit of acid solution, aluminum could promote the decomposition of H_2O_2 [23]; (2) too high Cl-doping content might block the contact between aluminum and Gr, reducing the intergranular corrosion and galvanic corrosion of aluminum.

3.2.2. Role of N-doping

Fig. 2d displayed the production of H_2O_2 of Al-Gr composite with/without N-doping. The accumulation concentration of H_2O_2 in Cl-Al-Gr/O_2 system within 120 min is only 14.9 mg/L, which was lower than that in Cl, N-Al-Gr/O_2 system (813.9 mg/L), suggesting that N-doping boosted the production of H_2O_2. Combined with the XPS results (Fig. 1g), the N-doping led to the high content of nitrogen active sites (AlN, pyridine N, pyrrolic N and graphitic N). The introduction of nitrogen active sites promoted the activity and selectivity for H_2O_2 production in ORR process because they could decrease the free energy of O_2 and pyrrolic N and graphitic N could decrease overpotential toward H_2O_2, which was confirmed by our previous work [1].

Fig. 2d also showed that Al-Gr composite without Cl, N co-doping had poor performance for H_2O_2 production in ORR process, indicating Cl, N co-doping played a key role in improving the activity of Al-Gr composite for H_2O_2 production.

3.2.3. Effect of initial pH

The solution pH played an important role in the production of H_2O_2. As can be seen (Fig. 3a) that the highest accumulation concentration of H_2O_2 after 120 min (813.9 mg/L) was achieved in the initial pH of 9, indicating that weak basic condition favored the production of H_2O_2. This might be related to that too acidic or too basic condition increased

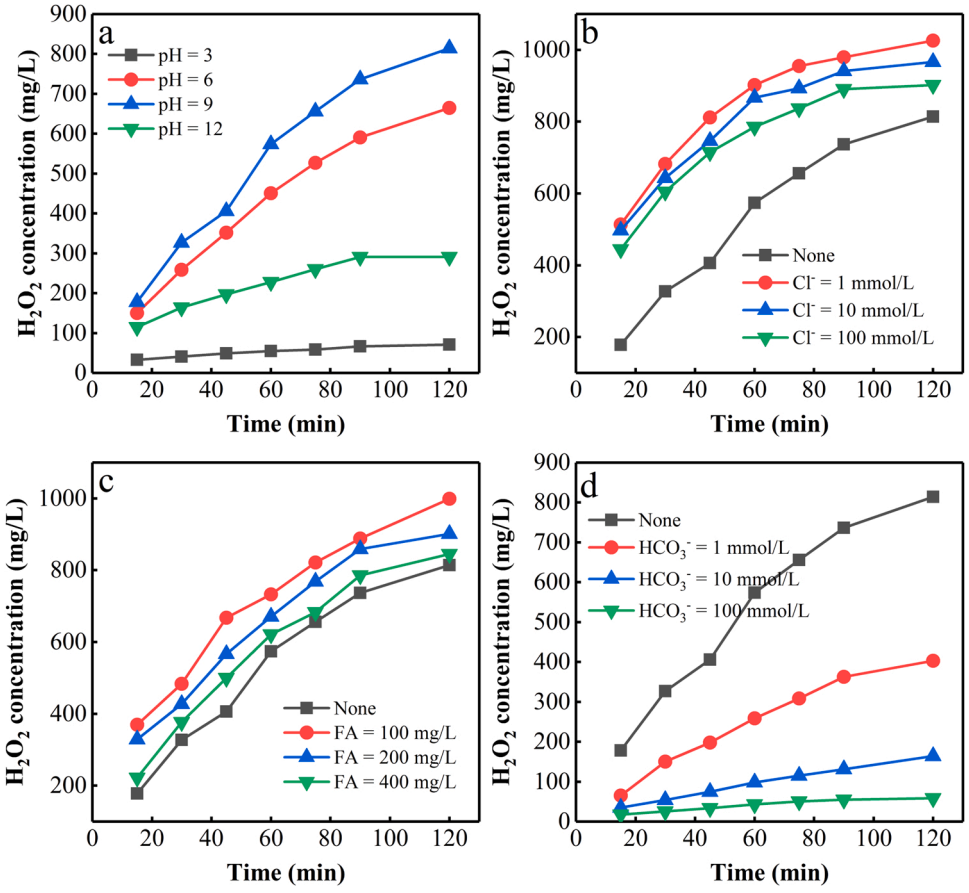

Fig. 3. Effects of initial pH (a), Cl^- concentration (b), fulvic acid concentration (c) and HCO_3^- concentration (d) on production of H_2O_2. Except for the investigated parameter, other parameters were set as follows: initial pH = 9, T = 20 °C, Cl, N-Al-Gr dosage = 2 g/L, O_2 flow rate = 400 mL/min.

the hydrogen-type corrosion of Al and accelerated the decomposition of H_2O_2. The higher production yield of H_2O_2 in initial pH 9 than that in initial pH 6 might be attributed to that there were a lot of formation of Al^{3+} species in the Cl, N-Al-Gr/O_2 process, which could induce the generation of H^+ by the hydrolysis, the generated of H^+ in initial pH 9 could more meet the requirement of O_2 activation than that initial pH of 6. This result was consistent with our previous works [23,26,27]. Although initial pH 9 was the optimum for H_2O_2 production, the high accumulation concentration of H_2O_2 was still obtained at other initial pH, suggesting that Cl, N-Al-Gr/O_2 process was suitable for wastewater treatment with different initial pH values.

3.2.4. Effect of coexisting substances

It was proved that a lot of Cl^-, fulvic acid (FA) and bicarbonate (HCO_3^-) existed in the landfill leachate [1,8,14,50], which might affect the generation of H_2O_2 by Cl, N-Al-Gr/O_2 process. Fig. 3(b-d) shows the production of H_2O_2 in the presence of Cl^-, FA and HCO_3^-, respectively. The accumulation concentration of H_2O_2 after 120 min increased to 1026.2 mg/L in the presence of 1 mmol/L Cl^-, while it decreased to 902.1 mg/L when Cl^- dosage increased from 1 to 100 mmol/L, which might be due to that a small amount of Cl^- promoted the electron donating rate of aluminum through pitting, while excessive Cl^- would lead to sharp acidification in the corrosion hole, which resulted in the competition of hydrogen evolution corrosion with the ORR [51]. Despite all these, Cl^- promoted the H_2O_2 production in the range of investigated Cl^- concentration in this study. The promotion of FA on the H_2O_2 production was also found in this work, although this effect decreased at high concentration. Fig. 3d confirmed the adverse effect of HCO_3^- on the ORR performance of Cl, N-Al-Gr composite.

The possible reason might be that HCO_3^- promoted the hydrolysis of nascent aluminum ions and generated more aluminum oxide, hindering corrosion of aluminum. Moreover, the production of H_2O_2 by ORR process was a process of proton consumption. The HCO_3^- would compete with O_2 for proton in the solution, inhibiting the production of H_2O_2. Similar phenomenon was found in our previous works [1,23]. Despite different coexisting substances played different roles in ORR performance of Cl, N-Al-Gr composite, the ORR performance of Cl, N-Al-Gr composite in MBR effluent was affected by the interaction of coexisting substances.

3.3. Removal of organic pollutants in MBR effluent by hybrid CPF process

3.3.1. Removal of organic pollutants by coagulation process

In the Cl, N/Al-Gr/O_2 process, lots of corrosion cells were formed, using aluminum as anode and graphite as cathode, and the high redox potential difference (2.4 V) between aluminum and graphite provided several strong electron donors for the O_2. The H_2O_2 production from this micro-electrolysis process was due to the high selectivity of N-doping Graphite for 2-electron reduction of O_2 [1]. At the same time, the nascent aluminum ions were generated, which could be used a coagulant to remove organic pollutants through coagulation.

The pH had significant effects on the removal of organic pollutants due to the pH-dependence of corrosion of aluminum, coagulation of aluminum ions and generation of H_2O_2. As depicted in Fig. 4(a-c), the removal efficiency of TOC and color increased with increase of initial pH from 1 to 3, but it decreased when initial pH increased from 3 to 9. The highest removal efficiency of TOC and color was 51.8% and 91.1%, respectively, at initial pH of 3.

In order to further discuss the effect of pH on the removal of organic pollutants, the pH variation was determined at different initial pH, and it was found that the final pH stabilized at 6–9, suggesting the probable existence of aluminum hydrolysis. The hydrolysis products of aluminum were pH-dependence and different forms of Al (III) had different coagulation performance. At pH < 5, the majority of Al (III) was unhydrolyzed aluminum ions, which could complex with the hydroxyl and carboxyl groups of humic substances, and then it enhanced the

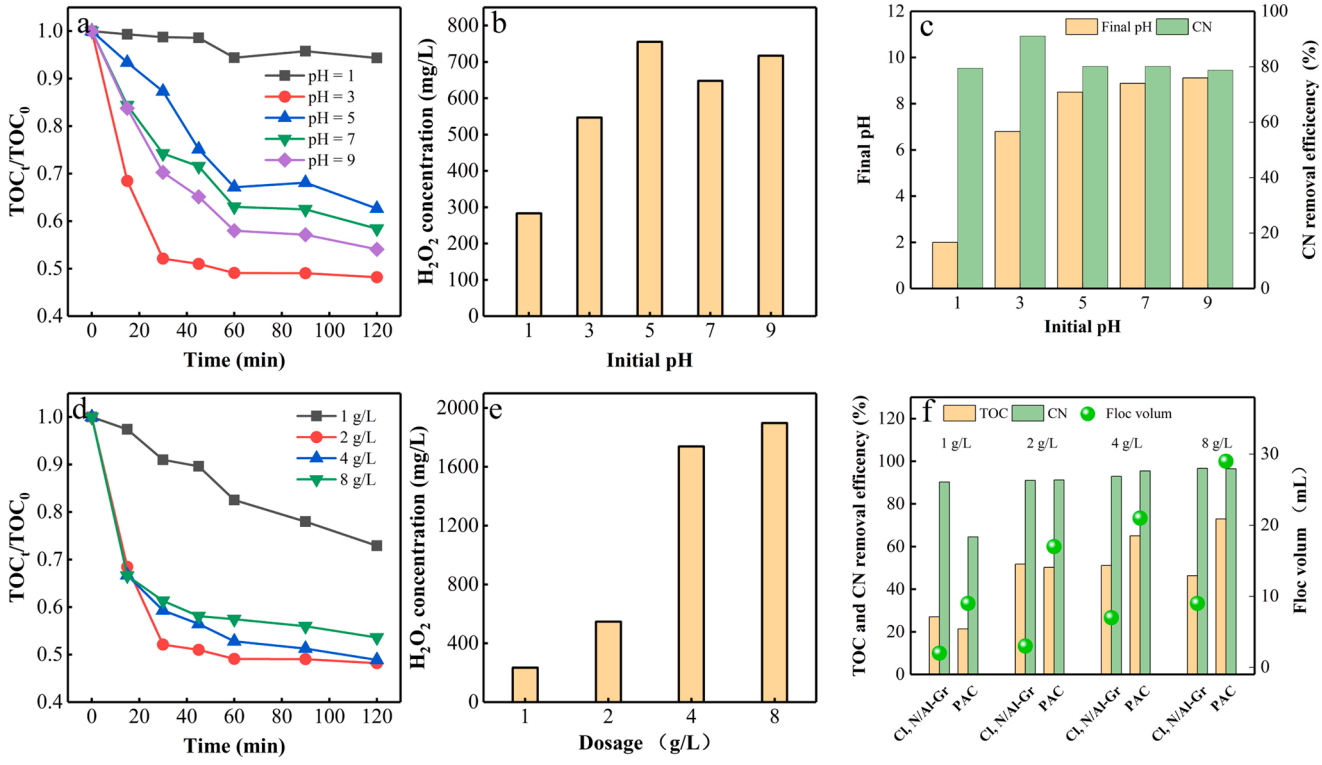

Fig. 4. The treatment of MBR effluent by Cl, N-Al-Gr/O_2 process: TOC removal at different initial pH (a), in-situ production of H_2O_2 at different initial pH (b), final pH value and CN removal (c) Reaction conditions: Cl, N-Al-Gr dosage = 2 g/L, T = 20 °C, O_2 flow rate = 400 mL/min; TOC removal at different Cl, N-Al-Gr dosages (d), in-situ production of H_2O_2 at different Cl, N-Al-Gr dosages (e) and removals of TOC and CN by different treatment processes(f). Reaction conditions: initial pH = 3, T = 20 °C, O_2 flow rate = 400 mL/min.

aggregation. At higher pH, hydroxyl complexes or polymers and aluminum hydroxide precipitates were the main form of Al (III), which favored the aggregation of organic pollutants by the action of incorporation of impurities and adsorption bridge.

When the initial pH was 3, the final pH stabilized around 8.5, suggesting that various Al (III) species would be produced in the ORR process at initial pH 3 due to aluminum hydrolysis. The highest removal efficiency of TOC and color was found at initial pH 3 might be owing to that these Al (III) species played synergistic effect on the removal of organic pollutants. Fig. 4b showed that the highest H_2O_2 yield was found at initial pH of 5. The possible reason for this might be that the H^+ from hydrolysis of Al^{3+} species in Cl, N-Al-Gr/O_2 process at initial pH 5 could more meet the requirement of O_2 activation than that initial pH of 3. Considering that the H_2O_2 yield at initial pH of 3 within 120 min was desired and the removal of organic pollutants was the main goal of coagulation process. Therefore, initial pH of 3 was selected in the subsequent experiments. Combined Fig. 4b with Fig. 3, the H_2O_2 yield in MBR effluent was no obviously different from that in aqueous solution under the same pH conditions, suggesting that the adverse effect of coexisting substances was negligible.

Fig. 4d shows that higher Cl, N-Al-Gr dosage resulted in a higher TOC removal efficiency and higher H_2O_2 yield at initial pH 3. However, when Cl, N-Al-Gr composite dosage was over 4 g/L, slight decreases of the TOC removal efficiency and insignificant boost of H_2O_2 production were observed. The reasonable explanation for this phenomenon was as follows: (1) the TOC removal in Cl, N-Al-Gr/O_2 process was mainly through the coagulation of the nascent aluminum ions, which removed the organic pollutants in leachate such as humic substances through the mechanism of charge neutralization and bonding bridging of Al-based species. The aluminum ions amount affected the coagulation removal of organic pollutants. As the dosage of Cl, N-Al-Gr increased over 4 g/L, the generated excess aluminum ions would cause surface charge reversal, thereby the electrostatic repulsion led to the deterioration of organic pollutants removal. Similar observations were reported for humic substances removal by aluminum salt coagulation processes [52, 53]; (2) The H_2O_2 production in Cl, N-Al-Gr/O_2 process depended on the dosage of Cl, N-Al-Gr and the oxygen supply. When the Cl, N/Al-Gr composite dosing was over 4 g/L, the limited oxygen supply led to insignificant increase of H_2O_2 production.

Moreover, from an economic point of view, 51.1% of TOC removal efficiency and 1739.2 mg/L accumulation concentration of H_2O_2 was enough for our desired outcome. The coagulation effluent from Cl, N-Al-Gr/O_2 process under the initial pH of 5, Cl, N-Al-Gr composite dosage of 4 g/L, reaction time of 120 min was therefore used in subsequent experiments.

The treatment of MBR effluent by polyaluminium chloride (PAC) was conducted at the initial pH of 5 (Fig. 4f). There was no obvious difference in the TOC removal between by Cl, N-Al-Gr/O_2 system and by PAC coagulation at the same dosage. However, the floc volume from the Cl, N-Al-Gr/O_2 system was far lower than that from PAC coagulation, suggesting that Cl, N-Al-Gr/O_2 process was a promising candidate for the removal of organic pollutants in MBR effluent.

3.3.2. *Removal of organic pollutants by Fe^{2+}/UVA process*

The degradation of organic pollutants in the coagulation effluent was examined at initial pH 1.5–7.0, UVA intensity of 50.01 mW/cm^2 and Fe^{2+} dosages of 12 mmol//L (Fig. 5a). In the presence of Fe^{2+} and UVA, the TOC removal efficiency within 120 min increased from 23.4% to 76.4% with the increase of initial pH from 1.5 to 5, while it decreased to 42.6% at initial pH 7, suggesting that initial pH of 5 was the optimum pH condition for the degradation of organic pollutants by Fe^{2+}/UVA process.

As shown in Fig. 5a, the TOC removal was positively correlated with the dosage of Fe^{2+}, the maximum removal of TOC (76.4%) was obtained at the Fe^{2+} dosage of 12 mmol/L. However, the TOC removal decreased when an excessive Fe^{2+} was used in Fe^{2+}/UVA process, which was because excessive Fe^{2+} in the presence of H_2O_2 could act as a scavenger for the formed •OH [37,54].

To explore the possible active species in Fe^{2+}/UVA process, EPR measurement was examined. As can be seen in Fig. 5(c-d), the characteristic peak of DMPO-•OH, DMPO-CO_2•$^-$ and DMPO-O_2•$^-$ EPR spectra were observed in the Fe^{2+}/UVA process, suggesting that •OH, CO_2•$^-$ and O_2•$^-$ were generated in the photo-Fenton process. In order to further identify the contributions of the active species to the degradation of organic pollutants in Fe^{2+}/UVA process, bisphenol-A as a probe pollutant and TBA, MV and BQ as •OH, CO_2•$^-$ and O_2•$^-$ inhibitors [26,37, 55], respectively were added in to the coagulation effluent, respectively. The degradation of bisphenol-A in the presence of different inhibitors by photo-Fenton process was investigated. Fig. 5e shows that all the inhibitors inhibited the degradation of bisphenol-A, suggesting the involvement of •OH, CO_2•$^-$ and O_2•$^-$ in the degradation of organic pollutions. Compared with MV and BQ, TBA exhibited the greatest inhibition degree, indicating that •OH played the main contribution to the degradation of organic pollutants.

To investigate the degradation mechanism of organic pollutants by photo-Fenton process. The removal of TOC in coagulation effluent by different processes were measured. As shown in Fig. 5f, TOC removal efficiency after 120 min in the presence of Fe^{2+} and in the presence of UVA were 37.6% and 32.1%, respectively, which might be attributed to the degradation of organic pollutants by •OH from the catalytic decomposition of H_2O_2 by Fe^{2+} alone and UVA alone, respectively. Compared with the Fe^{2+} alone and UVA alone, Fe^{2+}/UVA process achieved the highest TOC removal efficiency and H_2O_2 decomposition efficiency under the same reaction condition, suggesting the synergistic effect of Fe^{2+} and UVA for the H_2O_2 decomposition in the leachate.

It was reported that in photo-Fenton process, Fe^{3+} could be reduced into Fe^{2+} by UVA , which promoted the Fenton oxidation process [33, 55]. In order to discuss the recycle of Fe^{2+}/ Fe^{3+} by UVA in coagulation effluent, the evolution of Fe^{2+}/ Fe^{3+} concentration in the Fe^{2+}/coagulation effluent/UVA system and Fe^{2+}/coagulation effluent system were determined, respectively. Besides, the Fe^{3+} was added into the coagulation effluent and the ultra-pure water, respectively. The evolution of Fe^{2+}/ Fe^{3+} concentration under the UVA irradiation was also measured. As shown in Fig. 5(g-h), in the Fe^{3+}/coagulation effluent/UVA system and Fe^{3+}/ ultra-pure water /UVA system, Fe^{2+} concentration increased and Fe^{3+} concentration decreased with reaction time.

However, Fe^{2+} concentration in coagulation effluent was higher than that in ultra-pure water, suggesting that humic substances in coagulation effluent played an important role in the photo-reduction of Fe^{3+} into Fe^{2+}. In additional, the Fe^{3+} concentration in Fe^{2+}/coagulation effluent/UVA system was lower than that in Fe^{2+}/coagulation effluent system, indicating that UVA promoted the conversion of Fe^{3+} to Fe^{2+}. Combined with the above radical quenching test results, it can be concluded that humic substances in coagulation effluent could react with Fe^{3+} via LMCT mechanism with the regeneration of Fe(II) as well as the generation of CO_2•$^-$, which accelerated the H_2O_2 decomposition [24]. There were many reports on the formation of Fe(II) and CO_2•$^-$ from Fe^{3+} and carboxylic compounds such as oxalic acid and fulvic acid under light [33,35,55]. Our result was consistent with the literature.

Based on above results, it can be concluded that the highly efficient degradation of organic pollutants in coagulation effluent in the additional Fe^{2+} and UVA was attributed to that (1) there was high concentration of H_2O_2 in coagulation effluent, which could be decomposed into •OH with strong oxidizing capability by Fe^{2+} and UVA; (2) the humic substances in coagulation effluent promoted the regeneration of Fe^{2+} by LMCT mechanism, which enhanced the Fenton process as well as the degradation of humic substances [32]. Therefore, photo-Fenton process was high potential to the treatment of landfill leachate containing a large amount of humic substances.

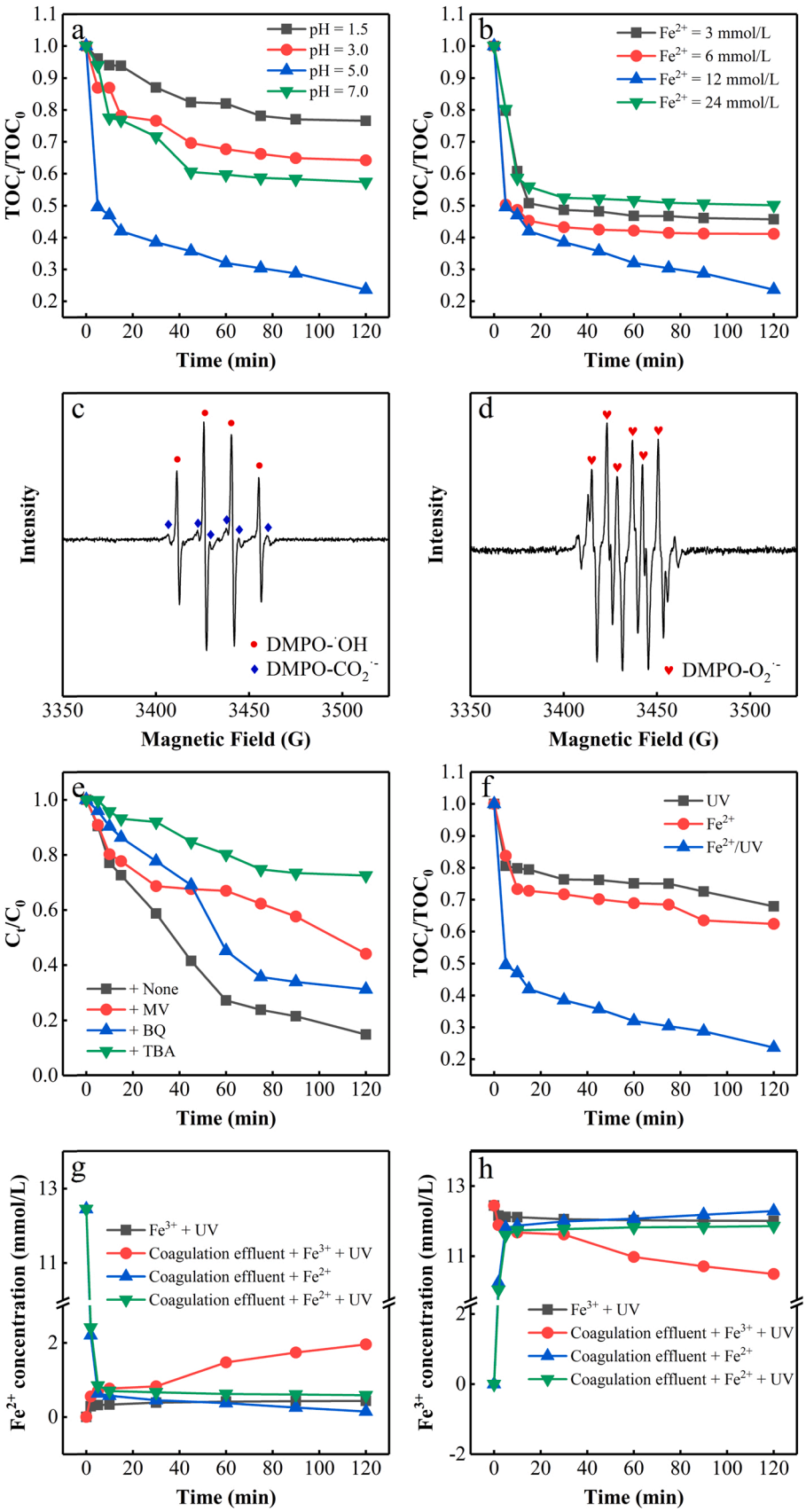

Fig. 5. The photo-Fenton oxidation of coagulation effluent by Cl, N-Al-Gr/O_2 process: TOC removal at different pH values (a), at different Fe^{2+}dosages (b) in the presence of free radical inhibitors (e) and in different systems(f), Except for the investigated parameter, other parameters were set as follows: initial pH = 5, T = 20 °C, Fe^{2+} dosages = 12 mmol/L, UVA intensity = 5.37 mW/cm^2. EPR spectra for DMPO-•OH, DMPO-CO_2•$^-$(c) and DMPO-O_2•$^-$ EPR (d) in Fe^{2+}/ coagulation effluent/ UVA system and the variation of iron ions (g, h). Experiment conditions: DMPO dosage = 100 mM, reaction time = 15 min.

3.3.3. Removal of organic pollutants by hybrid CPF process

Fig. 6(a-f) displayed the variation of TOC, color, apparent MW distribution and 3D-EEM spectra of organics in the MBR effluent, Cl, N-Al-Gr/O_2 coagulation effluent and Fe^{2+}/UVA effluent under optimal condition. TOC removal and color removal could be achieved 88.1% and 97.6% in this hybrid CPF process. Amor et al. [56] treated a mature landfill leachate by a combination of coagulation/flocculation with photo-Fenton process and found that about 75% DOC reductions was achieved at the coagulant dose of 2 g/L and H_2O_2 consumption of 116 mM. Vedrenne et al. [57] treated a mature landfill leachate using a coagulation/flocculation process followed by a photo-Fenton oxidation and found that the global removal efficiencies were 56% for the COD and 95% for color at an optimal dose of $FeCl_3$ of 300 mg/L and R ratio (R = $[H_2O_2]/[Fe^{2+}]$) of 114. Our result was higher or close to the reported results without addition of coagulant and H_2O_2, suggesting that the hybrid CPF process was a promising technology for the advanced treatment of landfill leachate.

The proportions of organics were 34.1% (< 500 Da), 40.4% (500 Da − 10 kDa), and 25.5% (>100 kDa) in MBR effluent, suggesting that high MW organic pollutants was the major components of organics in MBR effluent. Many researchers also found that the effluent from biological treatment of landfill leachate contained mainly high MW organic pollutants [14,22]. After Cl, N-Al-Gr/O_2 coagulation process, the organic pollutants with MW > 10 kDa and MW (500 Da-10 kDa) were decreased into 9.6% and 17.4%, respectively, indicating that Cl, N-Al-Gr/O_2 process favored the removal of high MW organic pollutants. Significantly, after Fe^{2+}/UVA process, organic pollutants with MW (500 Da − 10 kDa) was further decreased, while those with MW < 500 Da increased from 34.1% to 82.6%, which indicated that most large molecules of organics were degraded even mineralized. Generally, 88.2% removal of high molecular weight fractions (MW > 500 Da) in MBR effluent was achieved by hybrid CPF process.

During wastewater treatment, 3D-EEM spectra are widely used to characterize the fulvic acid and humic acid with the lEX (excitation wavelength)/lEM (emission wavelength) of (220−250)/(330−380) and lEX/lEM (250−330)/(380−480), respectively. As depicted in Fig. 6(d-f), similar EEM spectra were roughly obtained in the MBR effluent and coagulation effluent, indicating the existence of humic and fulvic acids [12,14,58]. The decrease of absorbance in coagulation effluent suggested the incomplete removal of humic and fulvic acids by coagulation and some humic-like substances were still remained in the coagulation effluent. After Fe^{2+}/UVA process, the absorbance sharply disappeared, indicating that humic-like and fulvic-like substances could be completely degraded [16].

3D-EEM spectra and MW distribution demonstrated that high MW fractions such as refractory fulvic-like substances in MBR effluent could be effectively removed during the hybrid CPF process, which should be attributed to the combination effect of coagulation and photo-Fenton oxidation.

Based on the structural characterization and the performance of production H_2O_2 by O_2 activation of Cl, N-Al-Gr and the MBR effluent treatment results by hybrid CPF process, the removal mechanism of organic pollutants by hybrid CPF process was proposed (Fig. 7).

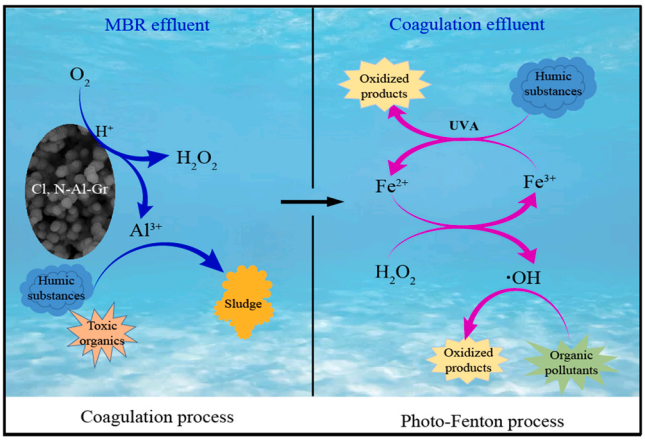

Fig. 7. The schematic diagram of organic pollutants degradation mechanism by hybrid CPF process.

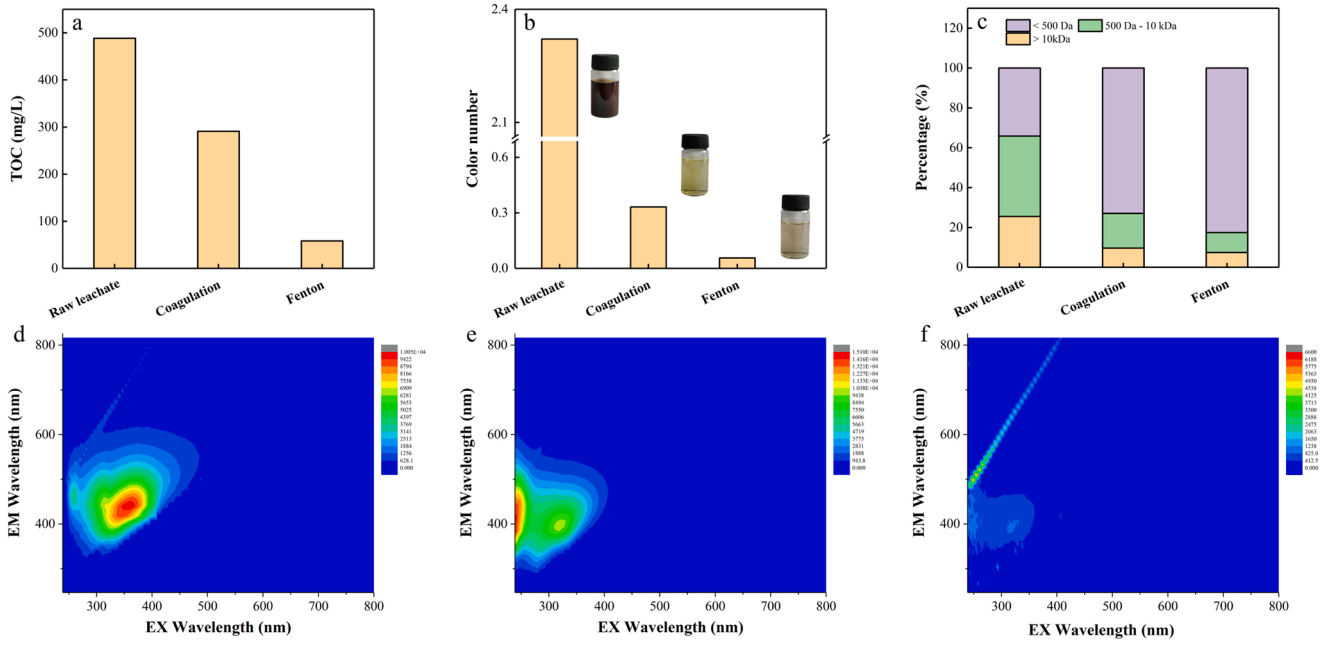

Fig. 6. Treatment efficacy of MBR effluent by hybrid CPF process: TOC removal (a), color removal (b), variation of apparent MW distribution (c), 3D-EEM spectra of MBR effluent (d), coagulation effluent, (e) and photo-Fenton effluent (f). Reaction conditions: in the coagulation process, initial pH = 3, Cl, N-Al-Gr dosage = 4 g/L, O_2 flow rate = 400 mL/min; in the photo-Fenton oxidation process, initial pH = 5, T = 20 °C, Fe^{2+} dosage = 12 mmol/L, UVA intensity = 5.37 mW/cm^2.

4. Conclusion

In the novel hybrid CPF process, Cl, N-Al-Gr/O_2 system could remove the refractory organic pollutants by coagulation at the same time in-situ produce H_2O_2, the produced H_2O_2 was then decomposed into •OH in the present of Fe^{2+} and UVA, which could efficiently degrade residual organics in the coagulation effluent. The fulvic-like substances in coagulation effluent could promote the degradation of organic pollutants by enhancing the regeneration of Fe^{2+} and the generation of CO_2•$^-$. 51.8% TOC removal and H_2O_2 concentration 1739.2 mg/L could be achieved by Cl, N-Al-Gr/O_2 process at Cl, N-Al-Gr composite dosage of 4 g/L, O_2 flow rate of 400 mL/min and initial pH 3. The subsequent photo-Fenton process resulted in removals of 76.4% TOC and 83.1% color at Fe^{2+} dosage of 12 mmol/L and initial pH of 5. Basically, 88.1% TOC removal efficiency and 97.6% color removal efficiency, 88.2% removal of high molecular weight fractions (MW $>$ 500 Da), efficient degradation of refractory fulvic-like substances were obtained from this novel hybrid CPF process under the optimal conditions without additional coagulants and H_2O_2. These results illustrated that hybrid CPF process is a promising and efficient technology for the advanced treatment of landfill leachate.

CRediT authorship contribution statement

Yong Liu: Formal analysis, Funding acquisition, Writing – review & editing, Supervision; **Yong Chen:** Investigation, Writing – original draft; **Yufeng Da:** Investigation; **Fei Xie:** Investigation; **Jianlong Wang:** Conceptualization, Funding acquisition, Methodology, Project administration, Supervision.

Declaration of Competing Interest

The authors declare that they have no known competing financial interests or personal relationships that could have appeared to influence the work reported in this paper.

Acknowledgements

The research was financially supported by the National Natural Science Foundation of China (51878427) and Applied Basic Research Project of Sichuan Science and Technology Department (2020YFG0158).

References

[1] Y. Liu, Y. Chen, J.H. Deng, J.L. Wang, N-doped aluminum-graphite (Al-Gr-N) composite for enhancing in-situ production and activation of hydrogen peroxide to treat landfill leachate, Appl. Catal. B 297 (2021), 120407.
[2] Y. Liu, J.L. Wang, Treatment of fresh leachate from a municipal solid waste incineration plant by combined radiation with coagulation process, Radiat. Phys. Chem. 166 (2020), 108501.
[3] Y.Y. Long, J. Xu, D.S. Shen, Y. Du, H.J. Feng, Effective removal of contaminants in landfill leachate membrane concentrates by coagulation, Chemosphere 167 (2017) 512–519.
[4] M.C. Nika, K. Ntaiou, K. Elytis, V.S. Thomaidi, G. Gatidou, O.I. Kalantzi, N. S. Thomaidis, A.S. Stasinakis, Wide-scope target analysis of emerging contaminants in landfill leachates and risk assessment using Risk Quotient methodology, J. Hazard. Mater. 394 (2020), 122493.
[5] Y.Z. Peng, S.J. Zhang, W. Zeng, S.W. Zheng, T. Mino, H. Satoh, Organic removal by denitritation and methanogenesis and nitrogen removal by nitritation from landfill leachate, Water Res 42 (2008) 883–892.
[6] M. Escola Casas, T.K. Nielsen, W. Kot, L.H. Hansen, A. Johansen, K. Bester, Degradation of mecoprop in polluted landfill leachate and waste water in a moving bed biofilm reactor, Water Res 121 (2017) 213–220.
[7] L. Joseph, Q. Zaib, I.A. Khan, N.D. Berge, Y.G. Park, N.B. Saleh, Y. Yoon, Removal of bisphenol A and 17alpha-ethinyl estradiol from landfill leachate using single-walled carbon nanotubes, Water Res 45 (2011) 4056–4068.
[8] L.M. Shao, Y.T. Deng, J.J. Qiu, H. Zhang, W.Y. Liu, K. Baziene, F. Lu, P.J. He, DOM chemodiversity pierced performance of each tandem unit along a full-scale "MBR+NF" process for mature landfill leachate treatment, Water Res 195 (2021), 117000.
[9] X.Z. Yi, N.H. Tran, T.R. Yin, Y.L. He, K.Y. Gin, Removal of selected PPCPs, EDCs, and antibiotic resistance genes in landfill leachate by a full-scale constructed wetlands system, Water Res 121 (2017) 46–60.
[10] M. El Kateb, C. Trellu, A. Darwich, M. Rivallin, M. Bechelany, S. Nagarajan, S. Lacour, N. Bellakhal, G. Lesage, M. Heran, M. Cretin, Electrochemical advanced oxidation processes using novel electrode materials for mineralization and biodegradability enhancement of nanofiltration concentrate of landfill leachates, Water Res 162 (2019) 446–455.
[11] F.C. Moreira, J. Soler, A. Fonseca, I. Saraiva, R.A. Boaventura, E. Brillas, V.J. Vilar, Incorporation of electrochemical advanced oxidation processes in a multistage treatment system for sanitary landfill leachate, Water Res 81 (2015) 375–387.
[12] H. Lin, H.J. Peng, X.W. Feng, X.J. Li, J.B. Zhao, K. Yang, J.B. Liao, D.M. Cheng, X. H. Liu, S.H. Lv, J.L. Xu, Q.G. Huang, Energy-efficient for advanced oxidation of bio-treated landfill leachate effluent by reactive electrochemical membranes (REMs): Laboratory and pilot scale studies, Water Res 190 (2021), 116790.
[13] B. Aftab, Y.S. Ok, J. Cho, J. Hur, Targeted removal of organic foulants in landfill leachate in forward osmosis system integrated with biochar/activated carbon treatment, Water Res 160 (2019) 217–227.
[14] W.M. Chen, Z.P. Gu, P. Wen, Q.B. Li, Degradation of refractory organic contaminants in membrane concentrates from landfill leachate by a combined coagulation-ozonation process, Chemosphere 217 (2019) 411–422.
[15] T. Guo, Y. Ji, J.W. Zhao, H. Horn, J. Li, Coupling of Fe-C and aerobic granular sludge to treat refractory wastewater from a membrane manufacturer in a pilot-scale system, Water Res 186 (2020), 116331.
[16] J. Xu, Y.Y. Long, D.S. Shen, H.J. Feng, T. Chen, Optimization of Fenton treatment process for degradation of refractory organics in pre-coagulated leachate membrane concentrates, J. Hazard. Mater. 323 (2017) 674–680.
[17] S.Y. Cheng, P.L. Show, J.C. Juan, J.S. Chang, B.F. Lau, S.H. Lai, E.P. Ng, H.C. Yian, T.C. Ling, Landfill leachate wastewater treatment to facilitate resource recovery by a coagulation-flocculation process via hydrogen bond, Chemosphere 262 (2021), 127829.
[18] M.S. Yusoff, H.A. Aziz, M. Zamri, F. Suja, A.Z. Abdullah, N.E.A. Basri, Floc behavior and removal mechanisms of cross-linked Durio zibethinus seed starch as a natural flocculant for landfill leachate coagulation-flocculation treatment, Waste Manag 74 (2018) 362–372.
[19] J.L. Wang, L.J. Xu, Advanced oxidation processes for wastewater treatment: Formation of hydroxyl radical and application, Crit. Rev. Environ. Sci. Technol. 42 (2012) 251–325.
[20] T.A. Kurniawan, W.H. Lo, Removal of refractory compounds from stabilized landfill leachate using an integrated H_2O_2 oxidation and granular activated carbon (GAC) adsorption treatment, Water Res 43 (2009) 4079–4091.
[21] J.L. Wang, J.T. Tang, Fe-based Fenton-like catalysts for water treatment: Preparation, characterization and modification, Chemosphere 276 (2021), 130177.
[22] L.Q. Wang, Q. Yang, D.B. Wang, X.M. Li, G.M. Zeng, Z.J. Li, Y.C. Deng, J. Liu, K. X. Yi, Advanced landfill leachate treatment using iron-carbon microelectrolysis-Fenton process: Process optimization and column experiments, J. Hazard. Mater. 318 (2016) 460–467.
[23] Y. Liu, J.R. Guo, Y. Chen, N. Tan, J.L. Wang, High-efficient generation of H_2O_2 by aluminum-graphite composite through selective oxygen reduction for degradation of organic contaminants, Environ. Sci. Technol. 54 (2020) 14085–14095.
[24] H.Y. Zhou, H. Zhang, Y.L. He, B.K. Huang, C.Y. Zhou, G. Yao, B. Lai, Critical review of reductant-enhanced peroxide activation processes: Trade-off between accelerated Fe^{3+}/Fe^{2+} cycle and quenching reactions, Appl. Catal., B 286 (2021), 119900.
[25] Y. Chen, Z. Yang, Y.B. Liu, Y. Liu, Fenton-like degradation of sulfamerazine at nearly neutral pH using Fe-Cu-CNTs and Al^0-CNTs for in-situ generation of H_2O_2/•OH/O_2•$^-$, Chem. Eng. J. 396 (2020), 125329.
[26] Y. Liu, N. Tan, J.R. Guo, J.L. Wang, Catalytic activation of O_2 by Al(0)-CNTs-Cu_2O composite for Fenton-like degradation of sulfamerazine antibiotic at wide pH range, J. Hazard. Mater. 396 (2020), 122751.
[27] N. Tan, Z. Yang, X.B. Gong, Z.R. Wang, T. Fu, Y. Liu, In situ generation of H_2O_2 using MWCNT-Al/O_2 system and possible application for glyphosate degradation, Sci. Total Environ. 650 (2019) 2567–2576.
[28] J.-C. Lee, Kurniawan, E.-Y. Kim, K.W. Chung, R. Kim, H.S. Jeon, A review on the metallurgical recycling of vanadium from slags: towards a sustainable vanadium production, J. Mater. Res. Technol. 12 (2021) 343–364.
[29] L.H. Shi, X.-W. Wang, M.-Y. Wang, J. Peng, C.X. Xiao, Extraction of molybdenum from high-impurity ferromolybdenum by roasting with Na_2CO_3 and CaO and leaching with water, Hydrometallurgy 108 (2011) 214–219.
[30] L.P. Fang, L. Xu, J. Deng, S.X. Gao, L.Z. Huang, Induced generation of hydroxyl radicals from green rust under oxic conditions by iron-phosphate complexes, Chem. Eng. J. 414 (2021), 128780.
[31] S.R. Kim, S. Kim, E.J. Kim, Photoreaction characteristics of ferrous oxalate recovered from wastewater, Chemosphere 249 (2020), 126201.
[32] J. Liu, J.J. Fan, T.Y. He, X.F. Xu, Y.L. Ai, H.R. Tang, H. Gu, T. Lu, Y.H. Liu, G. Liu, The mechanism of aquatic photodegradation of organophosphorus sensitized by humic acid-Fe^{3+} complexes, J. Hazard. Mater. 384 (2020), 121466.
[33] Y.W. Pan, Q. Wang, M.H. Zhou, J.J. Cai, Y.S. Tian, Y. Zhang, Kinetic and mechanism study of UV/pre-magnetized-Fe(0)/oxalate for removing sulfamethazine, J. Hazard. Mater. 398 (2020), 122931.
[34] J.L. Wang, S.Z. Wang, Reactive species in advanced oxidation processes: Formation, identification and reaction mechanism, Chem. Eng. J. 401 (2020), 126158.
[35] T.Y. Xu, Y.M. Fang, T.Y. Tong, Y.B. Xia, X. Liu, L.Z. Zhang, Environmental photochemistry in hematite-oxalate system: Fe(III)-Oxalate complex photolysis and ROS generation, Appl. Catal., B 283 (2021), 119645.

[36] R. Hong, L. Zhang, W. Zhu, C. Gu, Photo-transformation of atrazine in aqueous solution in the presence of Fe (3+)-montmorillonite clay and humic substances, Sci. Total Environ. 652 (2019) 224–233.
[37] Y. Liu, Q. Fan, J.L. Wang, Zn-Fe-CNTs catalytic in situ generation of H_2O_2 for Fenton-like degradation of sulfamethoxazole, J. Hazard. Mater. 342 (2018) 166–176.
[38] Y.Q. Huang, H.C. Liu, H.Y. Yuan, X.C. Lv, B. Xu, W.Z. Li, J. Uttaruean, X.L. Yin, C. Z. Wu, Migration and speciation transformation of K and Cl caused by interaction of KCl with organics during devolatilization of KCl-loaded model biomass compounds, Fuel 277 (2020), 118205.
[39] L. Yu, X. Ba, M. Qiu, Y.F. Li, L. Shuai, W. Zhang, Z.F. Ren, Y. Yu, Visible-light driven CO_2 reduction coupled with water oxidation on Cl-doped Cu_2O nanorods, Nano Energy 60 (2019) 576–582.
[40] Y.B. Wang, D. Meng, X. Zhao, Visible-light-driven H_2O_2 production from O_2 reduction with nitrogen vacancy-rich and porous graphitic carbon nitride, Appl. Catal., B 273 (2020), 119064.
[41] G. Lemes, D. Sebastián, E. Pastor, M.J. Lázaro, N-doped graphene catalysts with high nitrogen concentration for the oxygen reduction reaction, J. Power Sources 438 (2019), 227036.
[42] Y. Wang, H. Wu, Z. Sarossy, C.Q. Dong, P. Glarborg, Release and transformation of chlorine and potassium during pyrolysis of KCl doped biomass, Fuel 197 (2017) 422–432.
[43] H.B. Zhao, Q. Song, Q. Yao, Release and transformation of K and Cl during the pyrolysis of KCl-loaded cellulose, Fuel 226 (2018) 583–590.
[44] Z.X. Liu, Y.W. Ye, H. Chen, Corrosion inhibition behavior and mechanism of N-doped carbon dots for metal in acid environment, J. Clean. Prod. 270 (2020), 122458.
[45] T.X. Huong, Le, M. Bechelany, M. Cretin, Carbon felt based-electrodes for energy and environmental applications: A review, Carbon 122 (2017) 564–591.
[46] C.-Q. Pan, Q.-D. Zhong, J. Yang, Y.F. Cheng, Y.-L. Li, Investigating crevice corrosion behavior of 6061 Al alloy using wire beam electrode, J. Mater. Res. Technol. 14 (2021) 93–107.
[47] L. Yan, G.-L. Song, Z.M. Wang, D.J. Zheng, Crevice corrosion of steel rebar in chloride-contaminated concrete, Constr. Build. Mater. 296 (2021), 123587.
[48] J.R. Guo, Z. Su, J. Tian, J.H. Deng, T. Fu, Y. Liu, Enhanced hydrogen generation from Al-water reaction mediated by metal salts, Int. J. Hydrog. Energy 46 (2021) 3453–3463.
[49] Y.Z. Qian, H.W. Lai, J.F. Ma, G.J. Deng, B. Long, T. Song, L. Liu, X.Y. Wang, Y. X. Tong, Molten salt synthesis of KCl-preintercalated C_3N_4 nanosheets with abundant pyridinic-N as a superior anode with 10 K cycles in lithium ion battery, J. Colloid Interface Sci. 606 (2021) 537–543.
[50] C.B. Chen, H. Feng, Y. Deng, Re-evaluation of sulfate radical based-advanced oxidation processes (SR-AOPs) for treatment of raw municipal landfill leachate, Water Res 153 (2019) 100–107.
[51] J.L. Wang, S.Z. Wang, Effect of inorganic anions on the performance of advanced oxidation processes for degradation of organic contaminants, Chem. Eng. J. 411 (2021), 128392.
[52] P.K. Jin, J.N. Song, L. Yang, X. Jin, Selective binding behavior of humic acid removal by aluminum coagulation, Environ. Pollut. (Barking, Essex: 1987) 233 (2017) 290–298.
[53] Y.L. Kong, Y.Q. Ma, L. Ding, J.Y. Ma, H.W. Zhang, Z.L. Chen, J.M. Shen, Coagulation behaviors of aluminum salts towards humic acid: Detailed analysis of aluminum speciation and transformation, Sep. Purif. Technol. 259 (2020), 118137.
[54] Y. Liu, Z. Yang, J.L. Wang, Fenton/Fenton-like processes with in-situ production of hydrogen peroxide/hydroxyl radical for degradation of emerging contaminants: Advances and prospects, J. Hazard. Mater. 404 (2021), 124191.
[55] B.H. An, H.N. He, B.H. Duan, J.H. Deng, Y. Liu, Selective reduction of nitrite to nitrogen gas by CO_2 anion radical from the activation of oxalate, Chemosphere 278 (2021), 130388.
[56] C. Amor, E. De Torres-Socias, J.A. Peres, M.I. Maldonado, I. Oller, S. Malato, M. S. Lucas, Mature landfill leachate treatment by coagulation/flocculation combined with Fenton and solar photo-Fenton processes, J. Hazard. Mater. 286 (2015) 261–268.
[57] M. Vedrenne, R. Vasquez-Medrano, D. Prato-Garcia, B.A. Frontana-Uribe, J. G. Ibanez, Characterization and detoxification of a mature landfill leachate using a combined coagulation-flocculation/photo Fenton treatment, J. Hazard. Mater. 205–206 (2012) 208–215.
[58] W.X. Zhang, X.M. Li, Q. Yang, D.B. Wang, Y. Wu, X.F. Zhu, J. Wei, Y. Liu, L.H. Hou, C.Y. Chen, Pretreatment of landfill leachate in near-neutral pH condition by persulfate activated Fe-C micro-electrolysis system, Chemosphere 216 (2019) 749–756.